Supporting Online Material

Materials and methods

1. Genetic manipulation and cell culture

A vector containing the cAMP-sensor Epac1camps (*1*) was kindly provided by Dr. Martin J. Lohse and Dr. Viacheslav O. Nikolaev (University of Würzburg). The sequence encodes a cAMP binding domain of human Epac flanked by CFP and YFP. Binding of cAMP to the sensor protein equilibrates rapidly and can be detected fluorometrically as loss in FRET-efficiency (*1*). The entire open reading frame was PCR-amplified and ligated to the *Cla*I and *Xho*I sites in plasmid pA15GFP (*2*) whereby replacing GFP with Epac1camps to obtain an expression vector pA15Epac1camps. The construct allows constitutive expression of Epac1camps in *Dictyostelium discoideum* under the *act15* promoter. The wildtype axenic strain AX4 and *regA*- (*3*) was transformed by electroporation following a standard protocol (*4*) and selected clones were isolated for further analysis. Under a microscope, fluorescence of Epac1camps appears uniform in the cytosol with no apparent subcellular localization. Expression of full-length Epac1camps was also confirmed by Western blot using anti-GFP antibody (Clontech). The obtained clonal strains expressing Epac1camps developed and formed fruiting bodies indistinguishable from its parental strain AX4. One of these clonal strains was chosen based on the intensity and cell-cell uniformity of fluorescence and used for detailed analyses. A knock-out strain of the *pdsA* gene was prepared by homologous recombination using blasticidine as a selection marker in the Epac1camps/AX4 background. Cells were grown axenically in modified HL5 medium supplemented with 5% glucose, 40ng/mL vitamine B12, 80ng/mL folic acid, 1x antibiotic-antimycotic mix (Gibco) and 10μg/mL G418.

2. Protein purification and fluorometric measurements

A hexa histidine-tag was inserted directly on the N-terminus of the epac1camps sequence to obtain pA15His6x-Epac1camps. Typically 1-2x10^9 *Dictostelium discoideum* cells expressing the His6x- Epac1camps were washed and starved for 2hr. The cytosolic fraction was obtained by nitrogen decompression using a cell disruption vessel (model 4639l, Parr Instrument) followed by centrifugation. Protein was purified by affinity chromatography using nickel-sepharose resin (GE Healthcare). Concentrations were determined by Bradford's method using immunoglobulin as a standard. The typical yield was 0.4 mg per 1x10^9 cells. The protein was stored on ice and used within a few days. To obtain calibration curves, the purified protein mixed with cAMP or 8-Bromoadenosine-3',5'-cyclic monophosphate (8-Br-cAMP) was excited at 442nm and emission spectrum from 450nm to 600nm was measured at 22°C using a fluorometer (F-7000, Hitachi). For 8-Br-cAMP incorporation into the cells, washed cells were first incubated with 10 or 20mM caffeine for 40min. Cells were further incubated with 2mM DTT (Wako Chemical) and 0 to 20mM 8-Br-cAMP until the FRET signals reach a steady state (approximately 50 min). Cells were shaken at 22°C during the treatment. For time-lapse recording using the fluorometer, a continuously stirred cell suspension at 2x10^7cells/mL density was excited every 1min at 425nm and an emission spectrum between 470 to 530 nm was measured at a scanning speed of 1 nm/msec. To obtain dosage dependence in the change of FRET efficiency, the fluorescence intensities in images taken at 475 nm were divided by those from images taken at 525 nm to obtain relative intensity levels (fig. S3; y-axis). cAMP, 8-Br-cAMP and caffeine were obtained from Sigma. SQ22536 was obtained from Calbiochem.

3. Perfusion and cAMP stimulation

Vegetative cells were washed and shaken at 2x10^7 cells/mL in developmental buffer (DB; 10mM K/Na_2 phosphate buffer, 1mM $CaCl_2$, 2mM $MgCl_2$; pH 6.5) for 4 to 5h before

plating on a glass bottom dish (MatTek, Ashland, MA). Plates were allowed to sit still for 12 minutes while cells attach to the bottom. A chamber insert (35 mm diameter Wilco, Warner Instruments) mounted onto the dish using silicone grease (Dow Corning) served as perfusion device with a suction pump attached to the outlet. Two communicating syringe pumps (NE-1000X dual, New Era Pump Systems Inc., Wantagh, NY) attached to the inlet provided a constant influx of DB over a period of up to 2 hours. The chamber has a circular surface of 13 mm diameter with an average fluid volume of 0.25 ml. For cAMP stimulation, a gravity flow system with pinch valves (Warner Instrument) and C-tube fittings were used. Micropipette stimulations were performed by applying a method used for chemotaxis studies (*5*). A glass needle filled with 10μM cAMP and 0.1μg/μl Alexa594 was moved to the field of view by a motorized micromanipulator (NKII; Eppendorf) and pressurized at 80hPa using an injector (FemtoJet; Eppendorf). To remove the stimulus, pressure was released and the pipette was moved approximately 5mm away from the field of view.

4. Image Acquisition

Cells were observed at 22°C under an inverted epifluorescence microscope (IX81 Olympus, Japan) equipped with a Xenon lamp, an automated stage (Sigma Koki, Japan), filter wheels (Ludl) and oil immersion lenses (20x UplanSApo NA 0.85 and 60x PlanApoN NA 1.42; Olympus). For FRET measurements, 435nm excitation filter (BP425-445HQ; Olympus) and 460-510nm (BA460-510HQ; Olympus) and 515-560nm (BA515-560HQ; Olympus) bandpass filters were used to detect fluorescence from CFP and YFP respectively. A dichroic mirror (DM450) separated emission from excitation. The fluorescent and transmitted light images were captured with a depth of 16 bit by a 512x512 pixels using an Electron Multiplying CCD (EMCCD) camera (Photometrix, Tucson, AZ). To minimize photodamage to the cells, neutral density filters were used to reduce the light intensity, and the exposure time was limited to 10-15 ms for 60x objective lens and 30-50 ms for 20x objective lens. Images were taken at 4 to 30s intervals for total durations of 0.5h to 20h. CFP and YFP images were taken in succession at approximately 200ms

interval. Data acquisition and time-lapse recording was controlled by Metamorph software (Universal Imaging, Media, PA). For small population observation (Fig. 1), washed cells were suspended at a density of ~10^8 cells/ml and a drop of <1 μL was spotted onto a surface of hydrophogic agar (*6*) using a microloader (Eppendorf), resulting in a total of 100-200 cells in a circular spot of ~400 μm in diameter.

5. Data analysis

Image analyses were performed using ImageJ (National Institutes of Health, Bethesda, Maryland) and custom plugins programmed in JAVA; or with MATLAB (MathWorks, Natwick, MA) and custom routines therein. Acquired images were binarized and cell masks were generated, representing regions of interest that correspond to individual cells or groups of cells. Changes in FRET-efficiency during cAMP-induced cAMP response occur uniformly in the cytosol without apparent spatial heterogeneities. The fluorescence intensity was averaged for individual cell masks to reduce noise, and the ratio of the CFP- and YFP- channels was calculated. To obtain a time-series, the mean of the first 10 time points was subtracted from the ratio which typically yields values between 0 and 0.1. To extract data from individual cells at high cell densities, we used custom-made cell tracking programs. When two or more cells met they were sorted by manual inspection. Pulsing rates were obtained by manual counting. In order to evaluate the relative output of an isolated cell for a given input stimulus over a time period *T*, we computed the time-integral of I_{485}/I_{540} given by

$$I_{cyt.cAMP}(T) = \frac{1}{T}\int_0^T \mathrm{I}_{485}(t)/\mathrm{I}_{540}(t)\mathrm{d}t,$$

where the stimulus is applied at t = 0. The input-output relation (Fig. 3C) was obtained from these datasets (fig. S9).

6. Verification of Epac-based FRET observation of cytosolic cAMP changes.

The Epac-based cAMP sensor combined with time-lapse fluorescence microscopy allows direct measurements of cytosolic cAMP in *Dictyostelium discoideum*. Under a submerged

condition, cells starved for 3 to 7 hours show synchronized oscillations of cytosolic cAMP at 6 to 7 minutes period at a monolayer cell density (fig. S1A). The period becomes longer (10 to 20 minutes) as cell density is lowered (fig. S2 left panels). Concomitant shifts in the signals from the YFP- and CFP- channels signify changes in FRET-efficiency (fig. S1A). The peaks appear as loss of FRET (the fluorescence from CFP increases relative to that from YFP) in accordance with the expected rise in cAMP. Figure S1B shows that the phase of the oscillations can be entrained by pulsatile application of extracellular cAMP; a well-known behavior resulting from the cAMP-induced cAMP production (cAMP relay response). The oscillations are not observed in strains expressing CFP or YFP only (data not shown), indicating that oscillations are not provoked by other physiological factors such as cytosolic pH which could result in spectral changes in CFP or YFP alone.

The population-level behavior can be studied quantitatively for cells suspended in buffer using a fluorometer (fig. S1C; see section 2). Using this setup, we checked that the observed changes in FRET efficiency reflect changes in the level of cytosolic cAMP. *Dictyostelium discoideum* has three enzymes that convert ATP to cAMP - adenylyl cyclases ACA, ACB and ACG each developmentally regulated with distinct roles (*7*) in the life-cycle. ACA is a plasma membrane bound adenylyl cyclase expressed during the first 7 hours of development. It is indispensable for the oscillations and waves (*8*). When SQ22536, a specific inhibitor of ACA (*7*), is applied at 1 to 2mM, the oscillations of cytosolic cAMP cease (fig. S1D). Treatment with 10mM caffeine, which also inhibits adenylyl cyclase activity in *Dictyostelium* (*7*), had a similar effect (fig. S1E). We also confirmed that the lowering of FRET-efficiency upon cAMP stimulation is due to synthesis of cytosolic cAMP by ACA. When cells are treated with 2 mM SQ22536 or 10 mM caffeine, the cAMP-induced response is diminished significantly (figs. S1F and S1G). Together, these observations confirm that the periodic changes in the FRET efficiency is due to changes in the level of cytosolic cAMP.

7. Estimation of the cytosolic cAMP levels.

From fluorometric measurements of cell suspensions we can obtain a quantitative and reliable estimate of the FRET efficiency change in a population. Here we employ this setup to estimate the absolute concentration of cytosolic cAMP. To determine the minimum and maximum of the sensor's dynamic range in the cytosol, cells were either inhibited from synthesizing cAMP or saturated with membrane permeable cAMP analogue. Specifically, to inhibit adenylyl cyclase, cells were treated for 40 min with 10 to 20 mM caffeine (fig. S1E), resulting in maximal reduction of the relative cytosolic fluorescence intensities (I_{475}/I_{525}). The caffeine treated cells were then allowed to incorporate 8-Br-cAMP - a cell permeable analogue of cAMP - at various concentrations in the presence of DTT. After the loading has reached a steady state (at about 50 min, as judged by the changes in FRET efficiency) the new fluorescence level of the cell suspsension was measured using a fluorometer (see section 2). The relative intensity obtained from the spectra can be fitted by a binding curve (yellow line) with the half-maximal change occurring at 0.48 (±0.09) mM 8-Br-cAMP (fig. S3A). The binding curve is comparable to the curves of purified Epac1camps protein for both cAMP and 8-Br-cAMP (fig. S3B and S3C; yellow lines). Under our conditions, the sensor protein has EC_{50} values of 2.55 (±0.19) μM for cAMP (see also (*1*); 2.4 μM) and 0.40 (±0.07) μM for 8-Br-cAMP. Figs. S3A and S3C reveal that the amount of 8-Br-cAMP in the cytosol is roughly 3 orders of magnitude lower than in the extracellular medium, possibly due to low permeability and intracellular degradation of 8-Br-cAMP.

Apart from differences in the EC_{50} values, the three dosage dependence curves (fig. S3A-C) follow the same sigmoidal function. This implies that the expected dosage dependence of the fluorescent probe for cAMP in live cells should follow the same curve as the one obtained for 8-Br-cAMP (fig. S3A) except that it should be shifted to match the EC_{50} value for cAMP. By assuming that the EC_{50} for cAMP is the same in vitro and in vivo, we can esitmate the sensor's dynamic range in live cells by knowing the maximal (no 8-Br-cAMP loading) and the minimal FRET efficiency (8-Br-cAMP loading to saturation) in caffeine treated cells.

The relative fluorescence intensity of the cell suspension $I(t)$ at time t depends on the absolute cytosolic cAMP concentration ($[cAMP]_{cyt}$), given by

$$I(t) = \frac{(I_{max} - I_{min})[cAMP]_{cyt}}{(EC_{50} + [cAMP]_{cyt})} + I_{min}.$$

Here, the relative intensity measured for caffeine treated cells with or without 20mM 8-Br-cAMP are substituted as I_{max} and I_{min} respectively. Figures S3D and S3E show two representative time-series where the y-axis now indicates the absolute level of cytosolic cAMP obtained by inverting the above equation. The average cytosolic cAMP levels during the first 2 hours of development remain relatively unchanged (fig. S3, D and E). The basal level of cytosolic cAMP during the first 4 hours of development is approximately 400nM on average, and the cytosolic cAMP pulses peak between 5 and 20 μM (fig. S3, D and E). These measured peak concentrations are comparable to the levels of intracellular cAMP measured previously by isotope dilution assays (*9*). However, we also detect basal levels that are slightly lower than the ones reported in earlier measurements which were between 400 nM to 2 μM (*10, 11*). Possibly additional cAMP resides in intracellular vesicles (*12*) which is not detected here. Nonetheless, the current estimate suggests that a large fraction of the intracellular pool of cAMP is in the cytosol, which is in good agreement with earlier reports (*13*).

8. Derivation of Phase equation

In order to understand the onset of the synchronized oscillations, we use a mathematical model that can quantitatively capture the relationship between the dynamics at the single-cell level and that of the population. We first introduce the equations that simulate the pulsatile response of isolated cells to external stimuli (Fig. 3) by following a framework of phase dynamics (*14*). Subsequently we will couple these equations with the aim to

obtain predictions for the cells' population behavior.

In a population of N_C cells, the level of cytosolic cAMP in the i–th cell can be approximated by the phase of the oscillations following

$$[\mathrm{cAMP}]_{\mathrm{cyt,i}} = \frac{(-A_{\max} + A_{\mathrm{bas}}) \cdot \sin\theta_{\mathrm{i}} + A_{\max} + A_{\mathrm{bas}}}{2} \qquad \text{(eq. S1)},$$

where $A_{\max}$=20μM and A_{bas}=0.4μM indicate the maximum and the minimum concentrations, respectively (see section 7). According to Winfree's theory (*14-16*), the phase equation for excitable and oscillatory elements take the form of

$$\frac{\mathrm{d}\theta_{\mathrm{i}}}{\mathrm{d}t} = \omega \cdot (1 + \Phi \cdot \Gamma(\theta_{\mathrm{i}}))$$

which describes a response of a cell to a perturbation Φ. $\Gamma(\theta)$ is the phase response curve (*14*) that defines whether, upon perturbation, the phase will advance or will be delayed depending on the state of the current oscillation. For the cAMP signaling response in *Dictyostelium*, the phase response curve has been well described in the form of $\Gamma(\theta) \propto -\sin\theta$ (*17*). A model equation can thus be written as follows;

$$\frac{\mathrm{d}\theta_{\mathrm{i}}}{\mathrm{d}t} = \omega \cdot (1 - \Phi([\mathrm{cAMP}]_{\mathrm{ext}}) \cdot c_{excite} \sin\theta_{\mathrm{i}}) + \eta_{\mathrm{i}} \qquad \text{(eq. S2)},$$

where $2\pi\omega$ =1/6 (min^{-1}) represents the intrinsic frequency (Fig. 3, D and E), and $[\mathrm{cAMP}]_{\mathrm{ext}}$ is the level of extracellular cAMP. Here, we adopt changes in the cytosolic cAMP level as the perturbation with respect to the extracellular cAMP level by taking $\Phi(y) = K/(y + K)$ (K = 400pM; Fig. 3C). In its current structure, this formulation defines only the dose-dependence. In order to describe the reaction rate, we introduced a proportionality constant c_{excite} which can be determined by fitting the input-output relation to the single cell

data from Fig. 3C using the expression

$$I_{cyt.cAMP}(T) = \frac{1}{T}\int_0^T [\mathrm{cAMP}]_{\mathrm{cyt}}(t)\mathrm{d}t,$$

where the stimulus is applied between t = 0 and T = 3 min (see fit in fig. S6B, and also section 5). This is done numerically after substituting eq. S2 into eq. S1. Lastly, the noise term η_i was fit by Gaussian white noise ($|\eta_i|$ = 0.002) so that spontaneous firings occur at a very low rate (~ 0.0007/min at $[\mathrm{cAMP}]_{ext}$ = 0), as observed experimentally in well-isolated cells (fig. S4). Converting this noise magnitude to a corresponding level of cAMP using the Wiener-Khinchin theorem, we see that fluctuations of 3.5% is added to the basal cytosolic cAMP level (i.e. 400nM ± 14nM), which is below the resolution of our measurements. Note that the addition of noise of this magnitude would increase extracellular cAMP only by ~0.07pM (see eq. S3 below). Without excitable dynamics, the noise term does little to increase the concentration of extracellular cAMP and is insufficient to generate the spontaneous cytosolic cAMP pulses.

The level of extracellular cAMP in a perfusion chamber under a well-mixed condition is determined by secretion and dilution. Assuming that secretion follows first-order kinetics at a rate c_{sec} per cell (*18, 19*),

$$\begin{cases} \dfrac{d[cAMP]_{ex}(\vec{x})}{dt} = c_{sec}[\mathrm{cAMP}]_{cy,i} - \dfrac{k}{V_T}[\mathrm{cAMP}]_{ex}(\vec{x}) & (\vec{x} \in \mathrm{cell}) \\ \dfrac{d[cAMP]_{ex}(\vec{x})}{dt} = -\dfrac{k}{V_T}[\mathrm{cAMP}]_{ex}(\vec{x}) & (\vec{x} \notin \mathrm{cell}) \end{cases}$$

where $\vec{x}$ denotes a position vector, k is the dilution rate (ml/min) and V_T is chamber volume. By taking the spatial average of the extracellular and intracellular variables over the chamber volume, we rewrite Eq. 1 with a more explicit representation for the effective synthesis term r;

$$\frac{\mathrm{d}[\mathrm{cAMP}]_{\mathrm{ext}}}{\mathrm{d}t} = \rho \frac{S_{\mathrm{T}} V_{\mathrm{C}}}{V_{\mathrm{T}} S_{\mathrm{C}}} c_{\mathrm{sec}} [\mathrm{cAMP}]_{\mathrm{cyt}} - \frac{k}{V_{\mathrm{T}}} [\mathrm{cAMP}]_{\mathrm{ext}} \quad \text{(eq. S3).}$$

The cell density ρ (in a Mono Layer unit) is given by $\rho \equiv N_C S_C/S_T$ where S_C and S_T, V_C are the surface areas of a cell and of the chamber, and the volume of a cell, respectively. $[\mathrm{cAMP}]_{\mathrm{cyt}} \equiv \frac{1}{N_{\mathrm{C}}} \sum_{\mathrm{i}=1}^{\mathrm{i}=N_{\mathrm{C}}} [\mathrm{cAMP}]_{\mathrm{cyt,i}}$ is the level of cytosolic cAMP averaged over all N_C cells in the chamber

Eqs. S2 and S3 constitute a model that determines the time course of cAMP at the population level. In addition, since the time scales of secretion (*18, 19*), c_{sec}^{-1}, and of extracellular degradation V_T/k (< 1min) are faster than the time scale of the intracellular dynamics (characterized by the period $2\pi/\omega \sim 6$ min), we can approximate $[\mathrm{cAMP}]_{\mathrm{ext}}$ by

$$[\mathrm{cAMP}]_{\mathrm{ext}} \approx \frac{V_{\mathrm{C}} S_{\mathrm{T}}}{S_{\mathrm{C}}} \frac{\rho}{k} c_{\mathrm{sec}} [\mathrm{cAMP}]_{\mathrm{cyt}} \qquad \text{(eq. S4),}$$

from the steady state approximation of eq. S3. Substituting eqs. S1, S3 and S4 into eq. S2, the collective dynamics of the cell population is given by

$$\frac{\mathrm{d}\theta_{\mathrm{i}}}{\mathrm{d}t} = \omega \cdot \left(1 - \frac{c_{\mathrm{excite}} K \sin\theta_{\mathrm{i}}}{K + \frac{V_{\mathrm{C}} S_{\mathrm{T}}}{S_C} \frac{\rho}{k} c_{\mathrm{sec}} \frac{1}{N_C} \sum_{\mathrm{j}}^{\mathrm{j}=N_C} \frac{(-A_{\max} + A_{\mathrm{bas}}) \sin\theta_{\mathrm{j}} + A_{\max} + A_{\mathrm{bas}}}{2}} \right) + \eta_{\mathrm{i}} \quad \text{(eq. S5).}$$

When the population variance of θ_i is negligible, the multi-body problem can be effectively reduced to a 1-body problem using a mean-field approximation (*20*) with $\frac{1}{\mathrm{N_C}} \sum_{\mathrm{i}=1}^{\mathrm{i}=\mathrm{N_C}} \sin\theta_{\mathrm{i}} \approx \sin\theta$. Summing up eq. S5 over all cells, we obtain the following

mean-field model for the population

$$\frac{\mathrm{d}\theta}{\mathrm{d}t} = \omega \cdot \left(1 - \frac{c_{\mathrm{excite}} K \sin\theta}{K + \frac{V_C S_T}{S_C} \frac{\rho}{k} c_{\mathrm{sec}} \frac{(-A_{\max} + A_{\mathrm{bas}}) \sin\theta + A_{\max} + A_{\mathrm{bas}}}{2}} \right) \qquad \text{(eq. S6).}$$

Together with eqs. S1 and S4, the 1-variable equation simulates the dynamics of both $[\mathrm{cAMP}]_{\mathrm{cyt}}$ and $[\mathrm{cAMP}]_{\mathrm{ext}}$.

Lacking an amplitude equation, this model cannot display damping of the cytosolic cAMP oscillations as observed in Fig. 3A and 3B. Instead, the present model is designed to simulate the minimal excitable/oscillatory switch necessary to understand the onset of the synchronized oscillations (Fig. 4).

9. Estimation of cAMP outputs and model validation

Here we compare the simulated levels of cAMP synthesis and secretion by the above chosen parameters to earlier biochemical measurements (*8, 9, 21, 22*). At the onset of the synchronized oscillations, $[\mathrm{cAMP}]_{\mathrm{cyt}}$ is at a basal level of ~400 nM, as determined by the fluorometer experiments described above. From Fig. 2C, $\rho/k \sim 10^{-3}$ and hence, using the steady state approximation of eq. S4,

$$[\mathrm{cAMP}]_{\mathrm{ext}} \approx \frac{\rho}{k} \frac{V_C S_T}{S_C} c_{\mathrm{sec}} [\mathrm{cAMP}]_{\mathrm{cyt}} \sim 3\,(\mathrm{pM}) \qquad \text{(eq. S7)}$$

is the minimum level of extracellular cAMP required to invoke a synchronized pulse (V_C = 1.1×10^{-12} *l*, S_T = 1.33 cm^2 and S_C = 1.3×10^{-6} cm^2). Here we have chosen a secretion rate per cell of c_{sec} = 3.6 (min^{-1}) which is higher than the earlier reported value of ~1 (min^{-1}) (*18, 19*) to fit our experimental data (fig. 4B). This adjustment can be justified

considering that these earlier reports assumed higher basal cAMP levels (~1 μM) than what we have measured to estimate the secretion rate.

Using eq. S3, the synthesis rate r in eq. 1 can be expressed as

$$r = \frac{V_T S_C}{S_T V_C} c_{sec} [\text{cAMP}]_{cyt} = 5.2 \text{ (nM/min)}, \qquad \text{(eq. S8)}$$

where $V_T = 0.25$ ml.

From eq. S7, we can estimate the amount of cAMP continuously secreted by an individual cell per unit time near the onset of the transition by

$$\begin{aligned} c_{sec}[\text{cAMP}]_{cyt} &\approx \frac{k}{\rho} \frac{[\text{cAMP}]_{ext} S_C}{S_T V_C} \\ &= \frac{k}{\rho} \frac{[\text{cAMP}]_{ext} S_C}{V_C S_T} \frac{6 \cdot 10^{23} \cdot V_C}{60} \quad \text{(molecules/(cell}\cdot\text{ sec))} \\ &= 5.7 \cdot 10^{12} \frac{k}{\rho} [\text{cAMP}]_{ext} \quad \text{(molecules/(cell}\cdot\text{ sec))}. \end{aligned}$$

Below the onset of synchronized oscillatory activity ($\rho/k \sim 10^{-3}$), $[\text{cAMP}]_{cyt}$ is at a basal level of ~400nM. Thus

$$\begin{aligned} c_{sec}[\text{cAMP}]_{cyt} &\approx 3.6 \cdot 400 \text{ (nM/min)} \\ &= 7.3 \cdot 10^3 \text{(molecules/(cell}\cdot\text{sec))}, \end{aligned}$$

which is comparable to estimated levels of basal ACA activity (1-5x10^3 molecules/cell·sec) (*23*). Above the onset, the level of extracellular cAMP expected from the model simulations is $[\text{cAMP}]_{ext}$ = 10 pM (data not shown). Hence $c_{sec}[\text{cAMP}]_{cyt} \approx 2.9 \cdot 10^4$ (molecules/(cell·sec)), which again compared to the reported ACA activity is well within the bounds of basal and maximal (8x10^4 - 2x10^5 molecules /cell·sec)

cAMP levels (*8, 21*). At higher ρ/k (~ 10^{-1}), i.e. when the period levels off at 6 min, simulated extracellular cAMP oscillates in the nanomolar range (Fig. 4A; 1/3ML) which agrees with the level of extracellular cAMP oscillations in a dense population (*9, 22*). Together, these estimations confirm that the amount of secreted cAMP, as simulated by our model parameters, agree well with the earlier biochemical studies.

10. Numerical calculations

Numerical calculations of the model were implemented by 4^{th}-order Runge-Kutta method in C language. The numerical input-output relation (fig. S6B) is computed using eqs. S1 and S2. Time courses for $[cAMP]_{cyt}$ and $[cAMP]_{ext}$ (Fig. 4A and 4C and fig. S6C) are sequentially calculated from eqs. S5 and S1. The frequency of $[cAMP]_{cyt}$ oscillations (Fig. 4B) is calculated numerically after the system has reached steady state. The blue and grey squares in Fig. 4B are obtained from numerical calculations using eq. S5 with noise strengths of $|\eta_i|=0.002$ and $|\eta_i|=0$, respectively.

Supporting Figures

Figure S1: Epac1camps serves as an indicator for cytosolic cAMP in *Dictyostelium discoideum.* Synchronized oscillations are observed in cells starved for 3 to 7 hours. (**A**) A representative data taken from ~65 cells in a monolayer of cells submerged in developmental buffer. Upper panel: average fluorescence intensities of CFP-channel and YFP-channel are shown in violet and orange respectively. Lower panel: the ratio of average fluorescence intensities in the CFP and YFP channel. (**B**) The oscillations can be entrained (lower panel) by pulsatile application of extracellular cAMP (upper panel). (**C-E**) The periodic behavior is also observed in suspended cells. The synchronized oscillations are suppressed by (D) 10mM SQ22536 (SQ) and (E) 10mM caffeine (CAF). (**F-H**) 10μM cAMP was applied at times indicated by black arrows. The cAMP-induced response is suppressed by (F) 10mM SQ22536 or (G) 10mM caffeine. (H) Addition of 2mM DTT also elicits transient increase in cytosolic cAMP. Fluorescence intensities were recorded under a microscope (A-B) or by a fluorometer (C-H). The cell density is at $2x10^7$cells/ml for (C-H).

Figure S2: Spontaneous oscillations in intact populations require extracellular PDE. Cells had been starved for 4h and washed for 3 min by perfusion before time-lapse imaging begins at t=0. Left panels show the typical periodic firing events observed in submerged conditions. In experiments shown in the right column, DTT is added at t = 1 min. Cell densities are 1/2 ML (2 upper rows) and 1/4 ML (lowest row). When DTT is applied to inhibit extracellular cAMP-phosphodiesterase (PDE) (*24*), cells respond with a transient rise in cytosolic cAMP followed by a slow relaxation to the basal level (right panels; also fig. S1H). This behavior can be attributed to elevated levels of extracellular cAMP due to inhibition of PDE, consistent with a similar observation based on isotope dilution (*24*). Secretion of cAMP therefore appears to be occurring regardless of whether the cells are pulsing or not (*19*). Note that the time it takes for the elevated cytosolic cAMP to return to the basal level is very long (>20 min). In addition, the average cytosolic cAMP level in individual cells remains elevated when cells are continuously exposed to micromolar cAMP concentrations (Fig. 3B). It appears that extracellular cAMP is still degraded albeit very slowly under the presence of DTT.

Figure S3: Fluorometeric measurements of purified Epac1camps and cell suspension provide direct quantification of the cytosolic cAMP concentrations. (**A**) Caffeine treated cells that had incorporated 8-Br-cAMP exhibit dose-dependent changes in FRET-efficiency. (**B-C**) Purified epac1camps was mixed with various concentrations of (B) cAMP and (C) 8-Br-cAMP. Error bars indicate standard deviation. (**D**,**E**) Time course of the cytosolic cAMP level after nutrient deprivation. The time-lapse fluorometric measurements were performed at a fast scanning speed of 1nm/sec in order to avoid phototoxicity. Due to the scanning speed, signal to noise ratio of the data is relatively low. Two samples are shown to represent the typical behavior. Calibration points I_{max} and I_{min} are obtained at a slow scanning speed as in (A-C) for duplicate samples at t =100-120 min (See Materials and methods 7).

Figure S4: Spontaneous bursts in well-isolated cells, exhibiting random pulses of cytosolic cAMP. Cells were placed in a perfusion chamber at a density of 1/5000 ML. Flow rate was 2 ml/min. Individual cells are represented by different colors. Near the end of the recordings, cells were stimulated with 10 nM cAMP which serves as a control (indicated by stars in black). Out of the six experiments shown that represents a total of 60 hours of such runs, two incidents of spontaneous firing (a rate of ~0.0007 per minute) can be recognized (marked by stars in color). When cells are exposed to sub-nanomolar cAMP ranging from 1 pM to 100 pM, the firing rate increases to ~0.005 per minute (see also Fig. 3A). In the absence of extracellular cAMP, except for these sporadic pulses, we never observed self-sustaining periodic pulses at the individual cell-level. This excludes a possibility that there are specialized cells that are autonomously oscillatory (17) which would entrain simply excitable cell-types

Figure S5: Cell-cell variability in the firing events at low cell densities (1/32 - 1/128ML). Colored curves represent the relative fluorescence intensity measured for individual cells in a population. Black dots show the population average. (**A-C**) Only a fraction of cells participate in the sporadic firing events near the critical value of ρ/k when the cell population is beginning to exhibit synchronized pulses. (**D-F**) At a slightly higher cell density, cells that remain quiescent are

still present even though pulses appear more frequently. Cell densities are (A,C) 1/64ML, (B) 1/128ML and (D-F) 1/32 ML. Flow rate is (A,D) 2ml/min, (B,E) 1ml/min and (C,F) 0ml/min. Note that only a sub-population of cells pulsed and that they are not well synchronized. Such behavior is in marked contrast to periodic pulses observed at higher cell densities where they appear significantly more uniform and synchronized (see Fig. 1C).

Figure S6: A phase model for the cytosolic cAMP dynamics. **(A)** A basic equation $d\theta/dt = \omega\cdot(1-\Phi\cdot\sin\theta)$ illustrates how excitation switches to oscillations in the model (eq. S2). Above $\Phi = 1$, a pair of stable (filled circle) and unstable (open circle) fixed points exist (black line shown for $\Phi = 1.2$). When perturbation is small, the system is not excited (green arrow). However, when perturbation of sufficient magnitude is applied, the oscillator passes through the unstable fixed point and rotates around a ring once before returning to the stable fixed point (red arrows). Oscillations appear when $\Phi < 1$, since $d\theta/dt$ is positive for an arbitrary θ indicating continuous increase in phase (black line for $\Phi = 0.7$). **(B)** The input-output relation computed for a single oscillator (eqs. S1 and S2) (dashed line) and the corresponding relation from the experiments (solid line; from Fig. 3C). The parameters are $A_{max} = 20\mu M$ and $A_{bas} = 0.4\mu M$, $K = 400pM$, $\omega = 2\pi/6$ (1/min) and $c_{excite}=1.01$. By chosing these parameters, the model serves as an automaton that simulates the pulsatile output of cAMP by an isolated cell for a given input of extracellular cAMP. **(C)** Discrete firing events by the individual cells (red dots) show how the synchronized oscillations arise from stochastic pulsing (upper panel; 200 representative cells are plotted). Color in upper panel indicates cytosolic cAMP level of individual cells. The percentage of cells that fire simultaneously increases as extracellular cAMP concentration rises (red line in lower panel), further promoting synchronous firing by an even larger fraction of cells which in turn adds to the extracellular cAMP level. This chain reaction finally gives rise to synchronous firing of the entire population (observed at 270 min; $\rho/k=10^{-2.8}$ and $N_C= 1000$). Blue line in lower panel indicates average cytosolic cAMP concentrations.

Figure S7: cAMP signal propagates in wave-like manner in small populations. Plotted below each time window from Fig. 1B is a representation of the cell population where the different regions are color-coded according to their respective pulsing times. At time zero, the first region pulsed,

corresponding to the left-most signal trace in the top row and to the black region in the bottom row. The longer it took for a region to pulse after that initial pulse, the lighter the color in the bottom row.

Figure S8: Stimulation experiments. (**A, B**) Individual cells responding to repetitive stimuli at 4 min (A) and 15 min (B) intervals. Stimuli are all at 10 nM for 1 min. The gray shaded regions indicate stimulus application; in white regions buffer is perfused without addition of cAMP stimulus. Cells were separated from each other by at least 1mm. The flow rate was 4 ml/min.

Figure S9: Representative data used to obtain the input/output relation in Fig. 3C. (**A**-**C**) cAMP-induced cytosolic cAMP signaling response. Representative time courses for isolated cells in a perfusion chamber. Cells are represented by different colors. The concentration of extracellular cAMP was changed at time points indicated by dashed lines.

Figure S10: Deletion of extracellular and intracellular PDEs. **(A)** Cells that do not produce extracellular PDE (*pdsA*-) are unable to oscillate synchronously without assisted removal of extracellular cAMP by perfusion (in contrast to the wild type cells in fig. S1A). Dashed line indicates time when washing with buffer at a rate of 4mL/min began (cell density; 1/2ML). **(B)** Isolated *regA*- cells exhibit the cell-intrinsic rhythmic activity when continuously stimulated by a glass needle filled with 10μM cAMP (Materials and methods 3). Dashed lines indicate time of application and removal of the stimulus.

Supporting References

1. **V. O. Nikolaev, M. Bunemann, L. Hein, A. Hannawacker, M. J. Lohse, *J Biol Chem* 279, 37215 (2004).**
2. **P. Fey, K. Compton, E. C. Cox, *Gene* 165, 127 (1995).**
3. **P. Thomason *et al.*, *EMBO J* 17, 2838 (1998).**
4. **W. Nellen, C. Silan, R. A. Firtel, *Mol. Cell. Biol.* 4, 2890 (1984).**

5. **X. Xu, M. Meier-Schellersheim, J. Yan, T. Jin, *J Cell Biol* 178, 141 (2007).**

6. **T. M. Konijn, *Experientia* 26, 367 (1970).**

7. **E. Alvarez-Curto, K. E. Weening, P. Schaap, *Biochem J* 401, 309 (2007).**

8. **H. Patel *et al.*, *EMBO J.* 19, 2247 (2000).**

9. **G. Gerisch, U. Wick, *Biochem. Biophys. Res. Commun.* 65, 364 (1975).**

10. **C. P. Klein, *FEBS Lett.* 68, 125 (1976).**

11. **M. B. Coukell, F. K. Chan, *FEBS Lett.* 110, 39 (1980).**

12. **P. W. Kriebel, V. A. Barr, E. C. Rericha, G. Zhang, C. A. Parent, *J Cell Biol* 183, 949 (2008).**

13. **C. D. Schoen, J. C. Arents, T. Bruin, R. van Driel, *Exp. Cell Res.* 181, 51 (1989).**

14. **A. T. Winfree, in *The geometry of biological time (Biomathematics series)*. (Springer-Verlag, New York, 1980).**

15. **Y. Kuramoto, *Chemical Oscillations, Waves, and Turbulence*. (Springer, Berlin, 1984).**

16. **E. M. Izhikevich, in *Dynamical Systems in Neuroscience: The Geometry of Excitability and Bursting, Chapter 10, Synchronization*. (MIT Press, Cambidge, 2007).**

17. **V. Nanjundiah, *Biophys. Chem.* 72, 1 (1998).**

18. **P. J. M. van Haastert, *J. Gen. Microbiol.* 130, 2559 (1984).**

19. **M. C. Dinauer, S. A. MacKay, P. N. Devreotes, *J. Cell Biol.* 86, 537 (1980).**

20. **L. P. Kadanoff, *Statistical Physics: Statics, Dynamics and Renormalization*. (World Scientific, 2000).**

21. **G. Gerisch, D. Malchow, *Adv. Cycl. Nucl. Res.* 7, 49 (1976).**

22. **K. J. Tomchik, P. N. Devreotes, *Science* 212, 443 (1981).**

23. **W. F. Loomis, C. Klein, P. Brachet, *Differentiation* 12, 83 (1978).**

24. **P. N. Devreotes, P. L. Derstine, T. L. Steck, *J. Cell Biol.* 80, 291 (1979).**

Gregor et al (2009) Figure S1

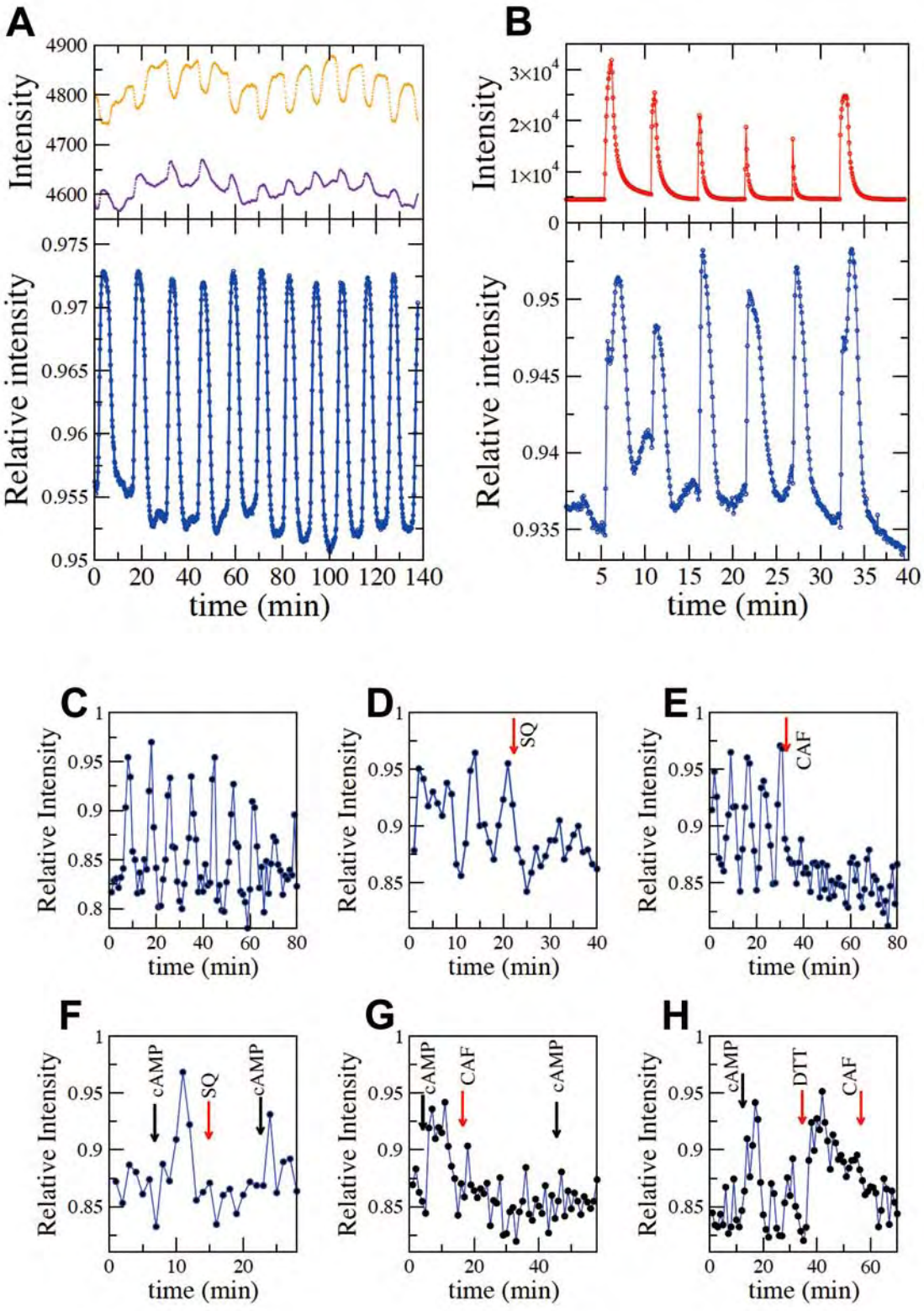

EMBARGOED UNTIL 2:00 PM US EASTERN TIME THURSDAY, 22 APRIL 2010

Gregor et al. (2009) Figure S2

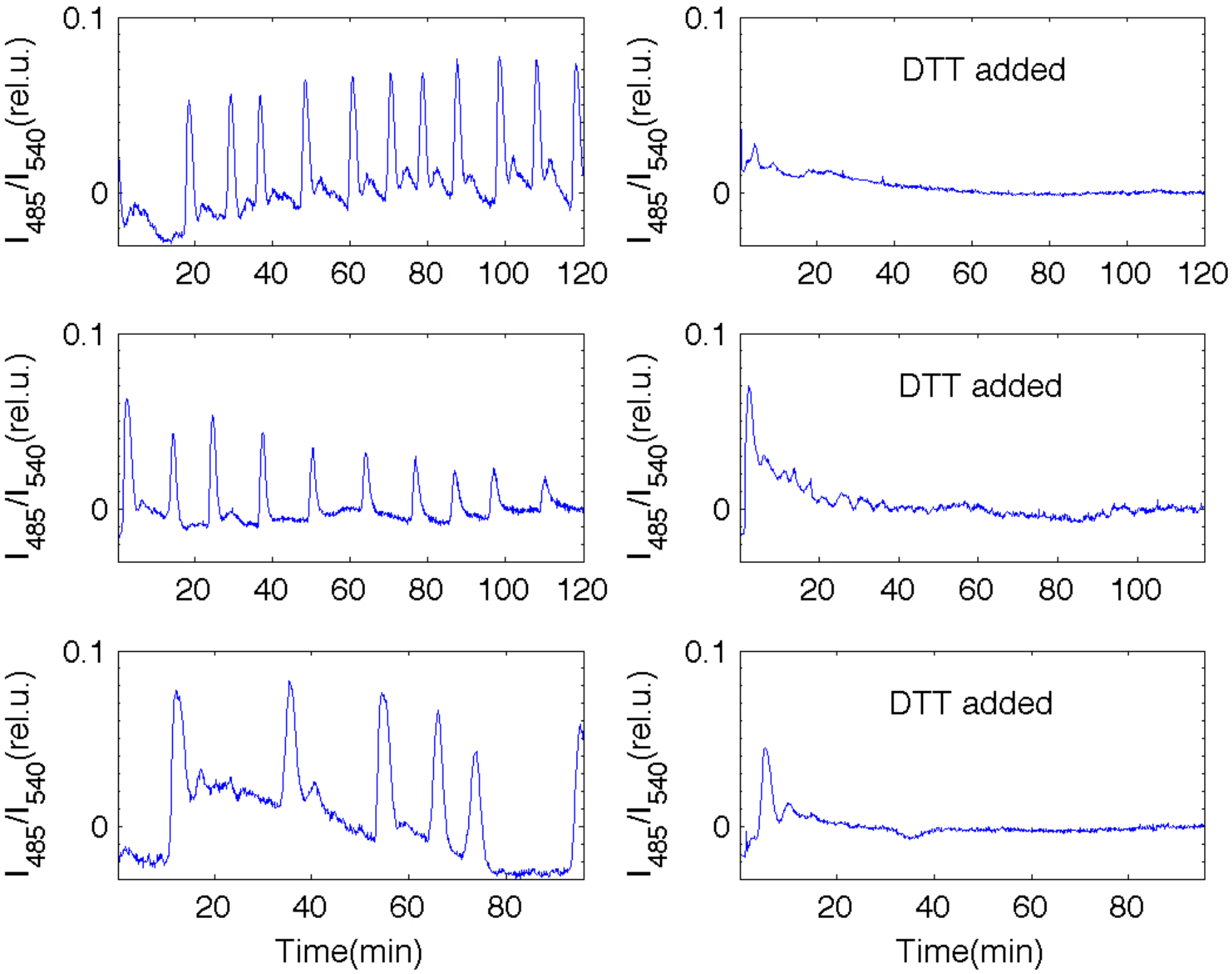

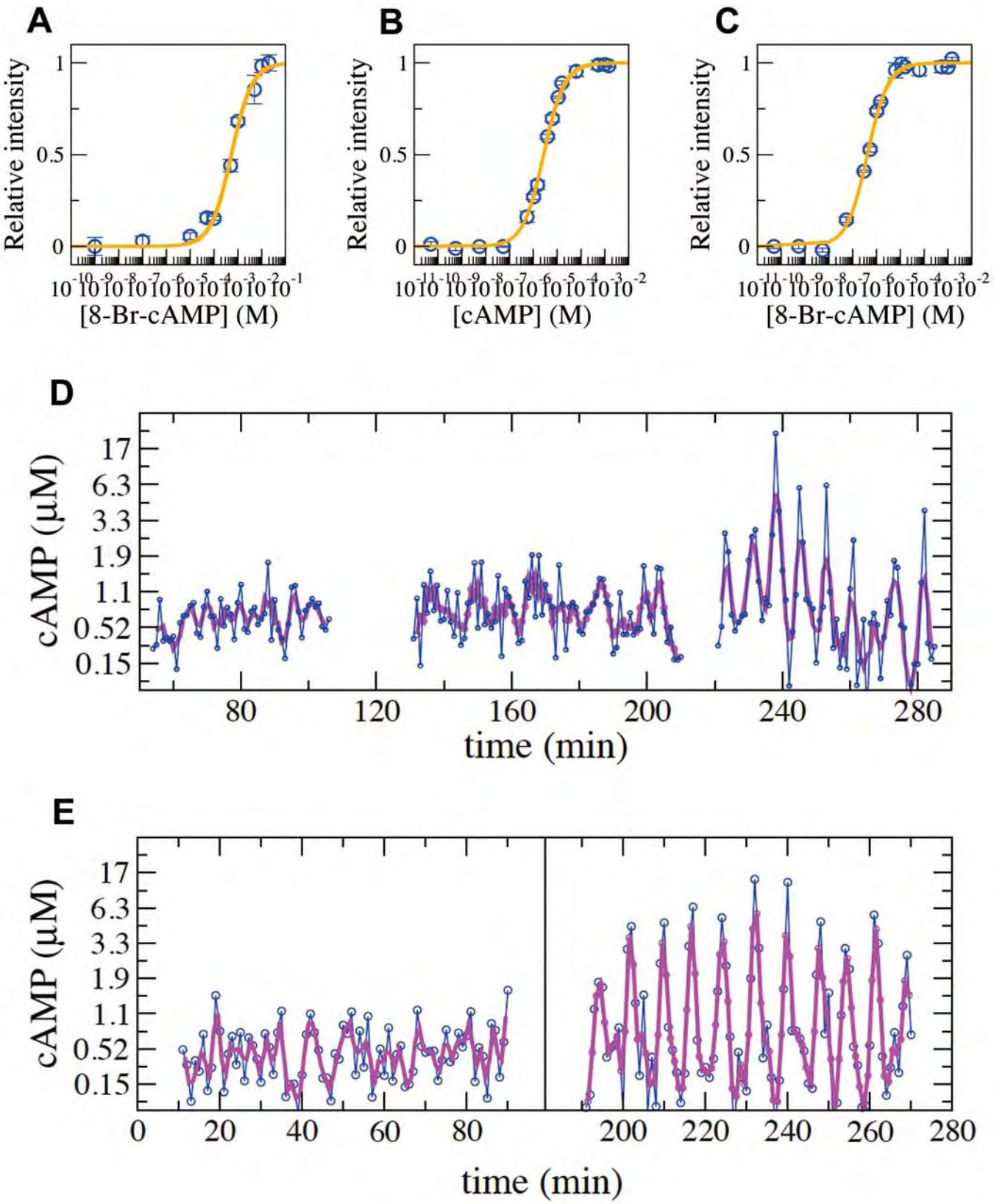

Gregor et al. (2009) Figure S4
EMBARGOED UNTIL 2:00 PM US EASTERN TIME THURSDAY, 22 APRIL 2010

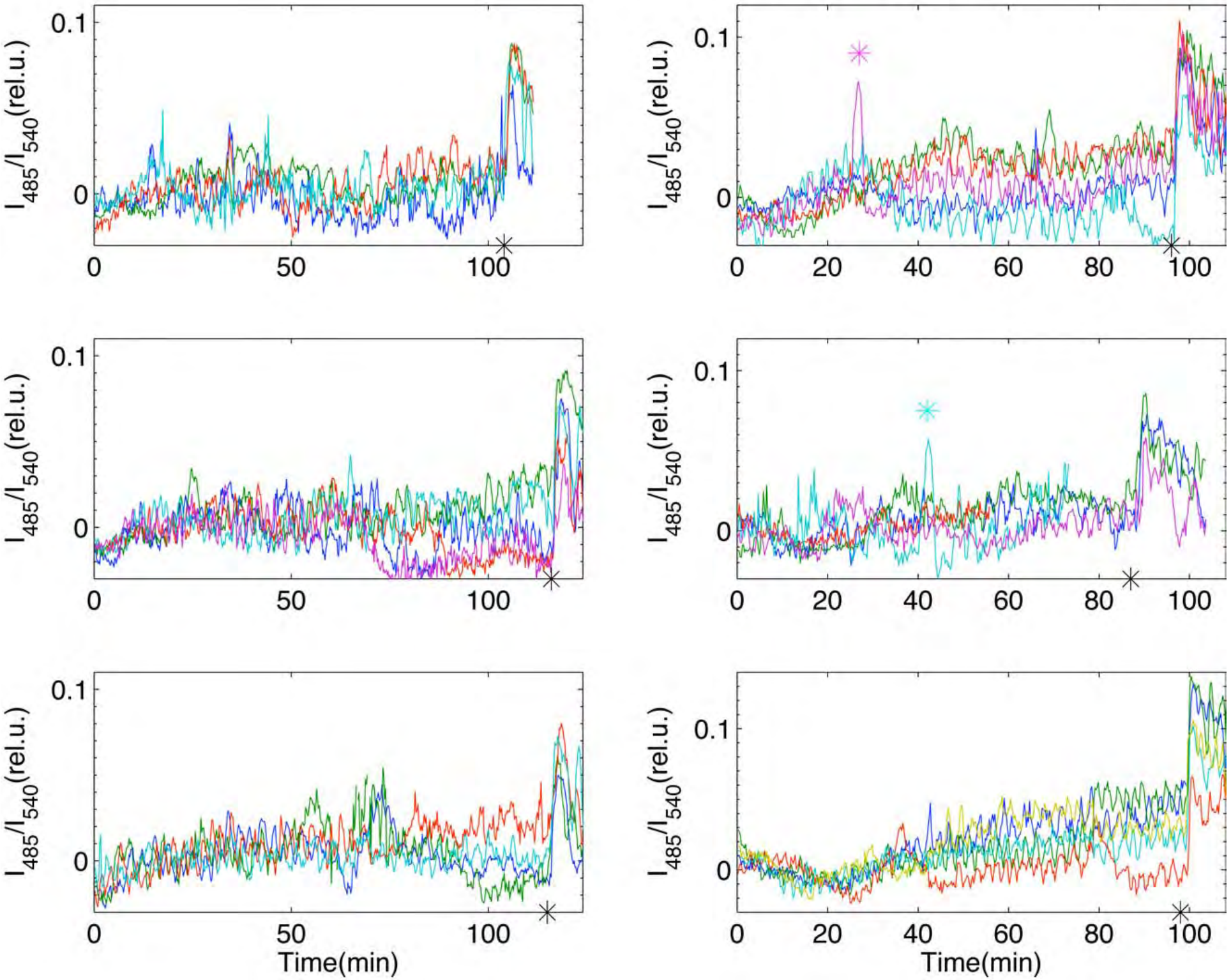

Gregor et al. (2009) Figure S5

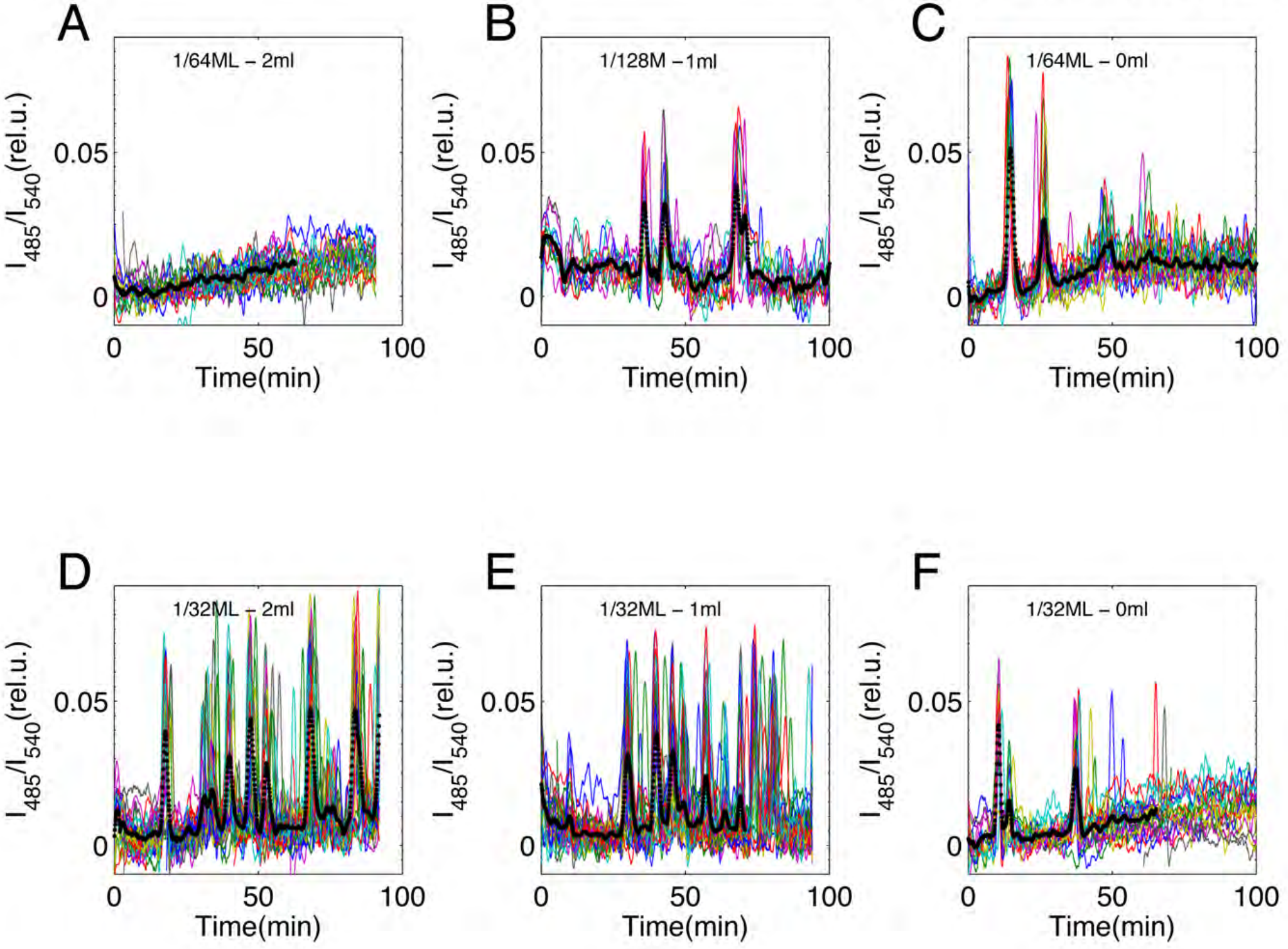

Gregor et al (2009) Figure S6

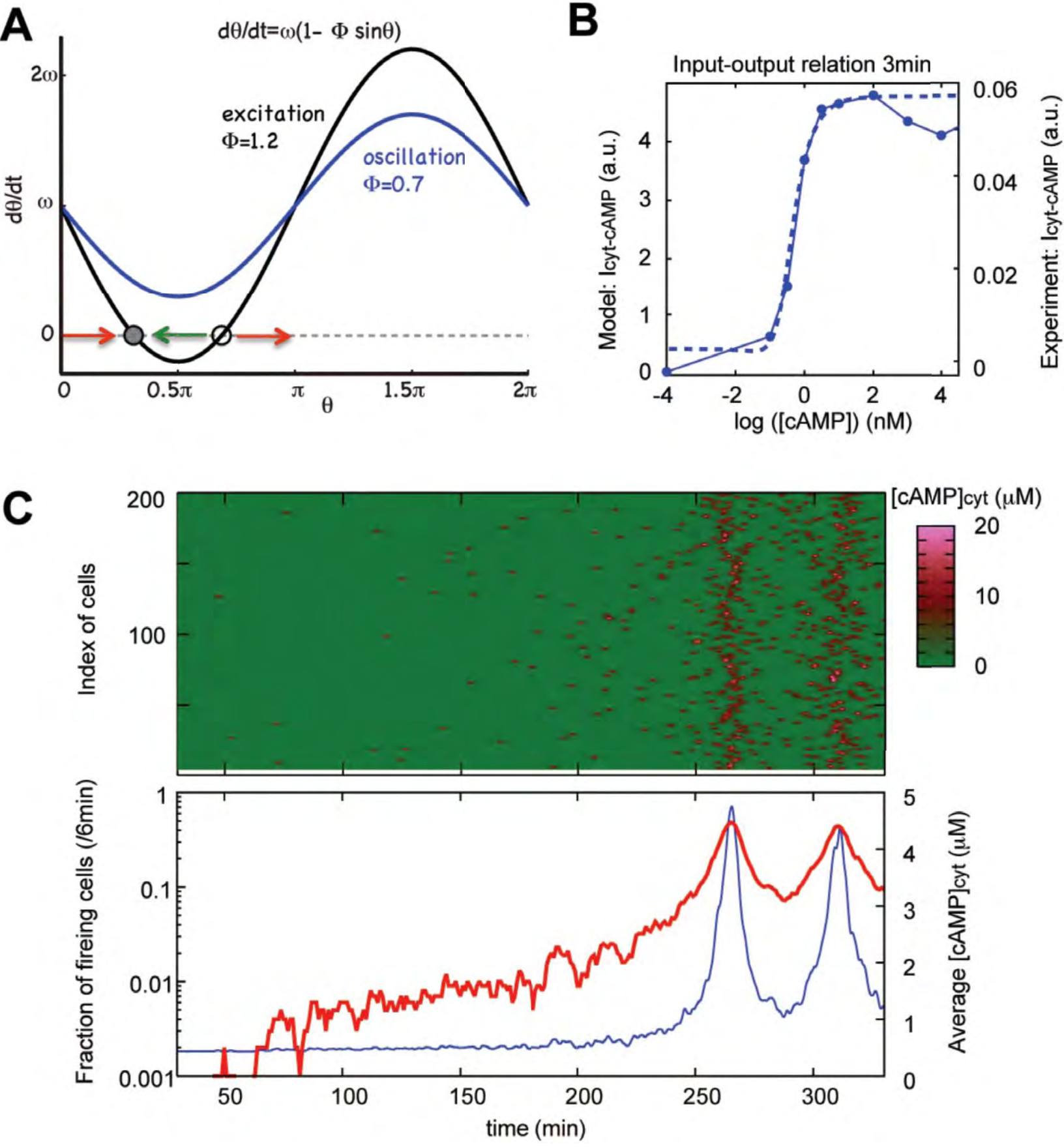

Gregor et al. (2009) Figure S7

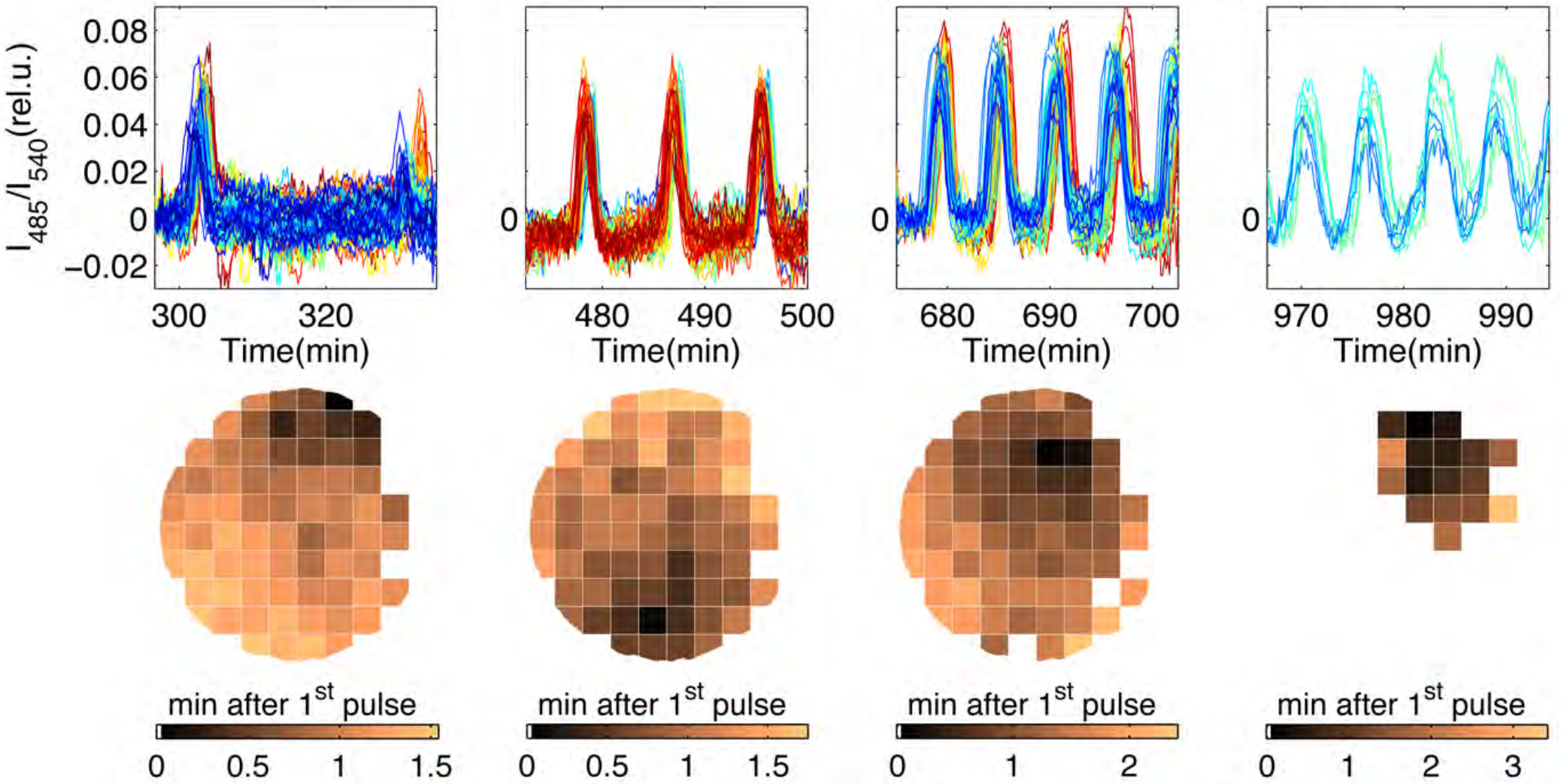

Gregor et al. (2009) Figure S8

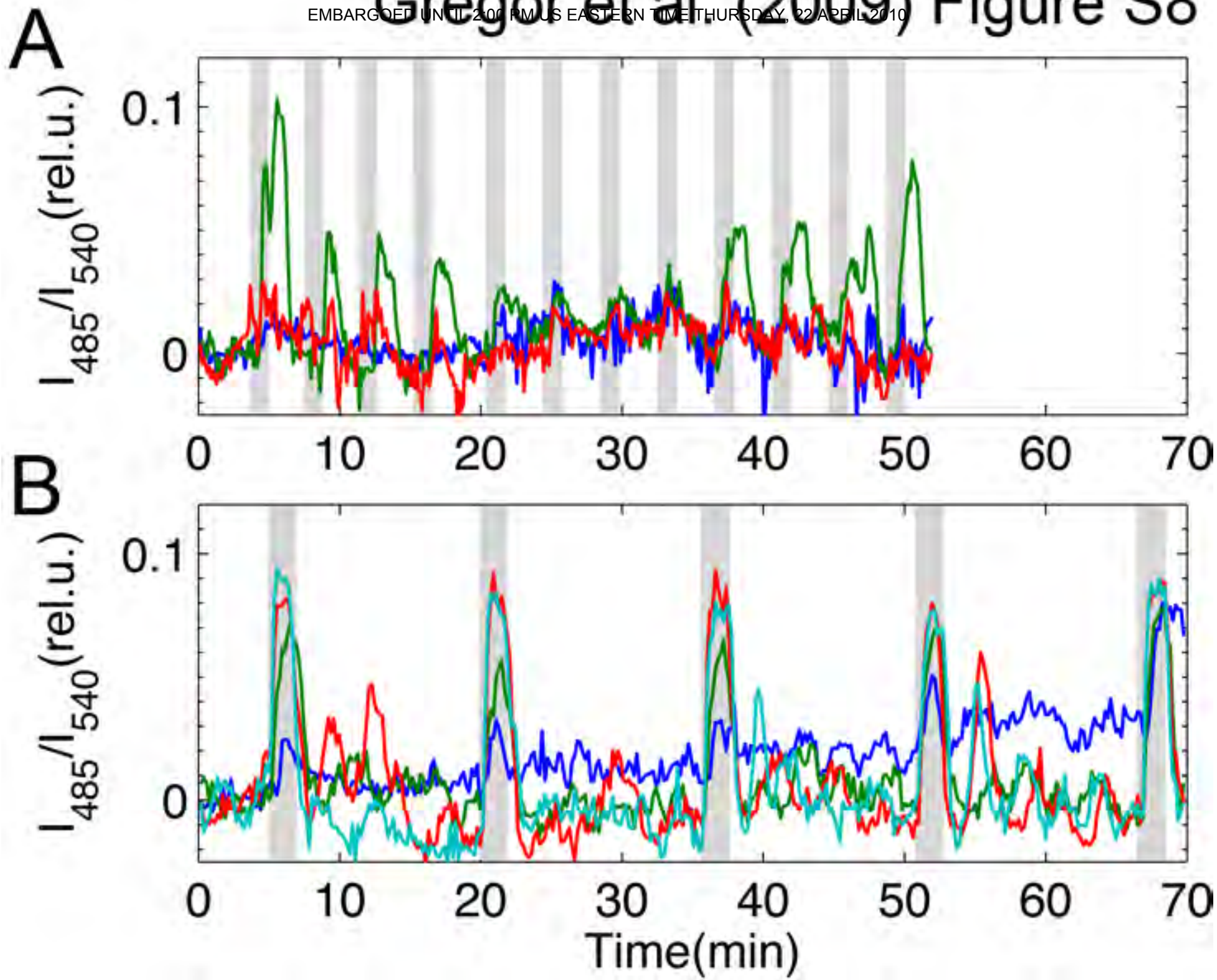

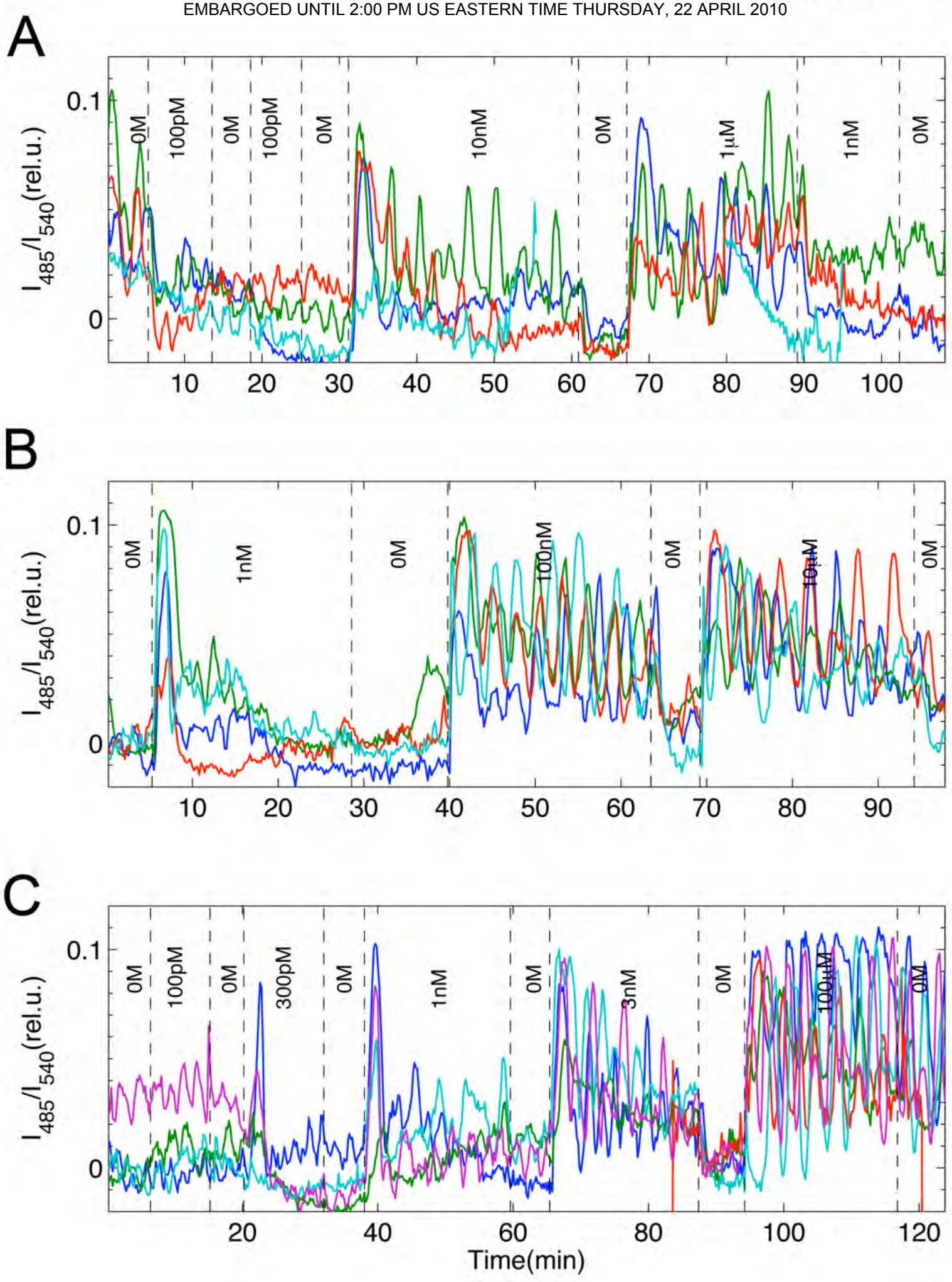

Gregor et al (2009) Figure S10